

Intracellular Determinants of Hippocampal CA1 Place and Silent Cell Activity in a Novel Environment

Jérôme Epsztein,^{1,2,3,4} Michael Brecht,¹ and Albert K. Lee^{1,5,*}

¹Bernstein Center for Computational Neuroscience, Humboldt University, Berlin 10115, Germany

²Institut de Neurobiologie de la Méditerranée, Marseille 13273, France

³Institut National de la Santé et de la Recherche Médicale U901, Marseille 13273, France

⁴Université de la Méditerranée Aix-Marseille II, UMR S901, Marseille 13273, France

⁵Howard Hughes Medical Institute, Janelia Farm Research Campus, Ashburn, VA 20147, USA

*Correspondence: leea@janelia.hhmi.org

DOI 10.1016/j.neuron.2011.03.006

SUMMARY

For each environment a rodent has explored, its hippocampus contains a map consisting of a unique subset of neurons, called place cells, that have spatially tuned spiking there, with the remaining neurons being essentially silent. Using whole-cell recording in freely moving rats exploring a novel maze, we observed differences in intrinsic cellular properties and input-based subthreshold membrane potential levels underlying this division into place and silent cells. Compared to silent cells, place cells had lower spike thresholds and peaked versus flat subthreshold membrane potentials as a function of animal location. Both differences were evident from the beginning of exploration. Additionally, future place cells exhibited higher burst propensity before exploration. Thus, internal settings appear to predetermine which cells will represent the next novel environment encountered. Furthermore, place cells fired spatially tuned bursts with large, putatively calcium-mediated depolarizations that could trigger plasticity and stabilize the new map for long-term storage. Our results provide new insight into hippocampal memory formation.

INTRODUCTION

The hippocampus is a key brain structure for learning and memory in mammals (Andersen et al., 2007). When a rodent explores a new space, a long-lasting (Thompson and Best, 1990) map (O'Keefe and Dostrovsky, 1971; O'Keefe and Nadel, 1978) defined by two classes of neurons rapidly appears (Hill, 1978; Wilson and McNaughton, 1993; Frank et al., 2004; Leutgeb et al., 2004) in its hippocampus. A place cell fires action potentials (APs) selectively whenever the animal is in a particular region—called the cell's place field—of the environment (O'Keefe and Dostrovsky, 1971), whereas silent cells fire few

APs across the entire area (Thompson and Best, 1989). In distinct mazes, different but partially overlapping subsets of CA1 pyramidal neurons have place fields (O'Keefe and Conway, 1978; Muller and Kubie, 1987; Thompson and Best, 1989; Leutgeb et al., 2005), with at least half of all neurons silent in each maze (Thompson and Best, 1989; Wilson and McNaughton, 1993). Thus, an environment is represented not only by where each place cell fires, but also by which cells are active versus silent there. Similarly, the human hippocampus represents specific items (Quiroga et al., 2005) or episodes (Gelbard-Sagiv et al., 2008) with unique and sparse (Waydo et al., 2006) subsets of active cells among a larger population of silent neurons.

Therefore, one of the most critical questions for understanding the formation of spatial memories in rodents as well as declarative memories in humans is—what determines which cells will form the memory trace of a given environment, item, or episode? Specifically, regarding rodents and space—what determines whether a given cell becomes a place cell versus a silent cell in a given maze? At a basic level, the possibilities include (1) differences in the amount and spatial distribution of synaptic input and (2) differences in intrinsic properties that shape the cell's response to inputs. Ultimately, for a neuron to have a place field, the membrane potential (V_m) by definition must consistently reach the AP threshold in a spatially selective manner. Conversely, V_m must generally stay below threshold for silent cells. But what precise combination of inputs and intrinsic properties achieves this (Figure 1)? For instance, both classes of cells could receive similar amounts of input but have different baseline V_m levels (e.g., Figures 1A versus 1B), or they could receive different amounts of input (e.g., Figures 1A versus 1C) or have different thresholds (e.g., Figures 1A versus 1D), with each such alternative having important implications for the origin of place and silent cells.

With the extracellular recording methods used in nearly all previous place cell studies, one can attempt to infer the input into a place cell based on its spiking output (Mehta et al., 2000); however, this is problematic for studying silent cells because they rarely spike. More importantly, extracellular methods cannot measure fundamental intracellular features such as the baseline V_m , AP threshold, or subthreshold V_m dynamics needed to reveal why spikes do or do not occur.

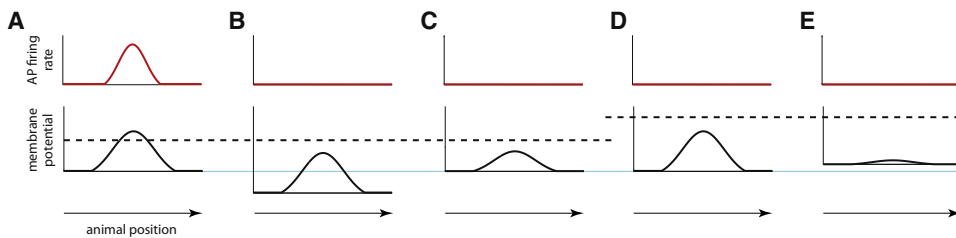


Figure 1. Spatial Distribution of Net Input and Intrinsic Cellular Properties Potentially Underlying the Difference between Place and Silent Cells in a Novel Environment

AP firing rate (red) and underlying membrane potential (V_m) at the soma due to input into cell (black) as a function of animal's location along a linear environment for place (A) and silent (B–E) cells. Baseline V_m (bottom of each V_m plot), baseline V_m of place cell (blue), and AP threshold (dashed).

(A) For a neuron to have a place field, V_m by definition must consistently reach spike threshold in a spatially selective manner.

(B–E) Conversely, V_m must generally stay below threshold for silent cells, but this could be achieved in many different ways. (B) Spatial tuning of input and amplitude of change in V_m due to input could both be same for place and silent cells but start from a lower baseline V_m in silent cells. (C) Baseline V_m and threshold could both be same for place and silent cells but the amplitude of change in V_m due to input could be smaller for silent cells. Note that smaller V_m change could occur in various ways such as a smaller net input or the same input acting on a neuron with lower input resistance (R_N). (D) Spatial tuning of input and amplitude of change in V_m due to input could both be same for place and silent cells but threshold could be lower in place cells. Other combinations of input pattern and intrinsic properties are possible. For instance, in (E), threshold is higher, baseline V_m is somewhat higher, and amplitude of change in V_m due to input and possibly spatial tuning of input are much lower in silent versus place cells.

But, recently, intracellular recording in freely moving animals has become possible (Lee et al., 2006, 2009; Long et al., 2010), and hippocampal place cells have been recorded intracellularly in both freely moving (A.K. Lee et al., 2008, Soc. Neurosci., abstract [690.22]; Epsztein et al., 2010) and head-fixed (Harvey et al., 2009) rodents, providing an opportunity to directly measure inputs and intrinsic properties during spatial exploration. Here, we used head-anchored whole-cell recordings in freely moving rats (Lee et al., 2006, 2009) as they explored a novel maze in order to investigate what underlies the distinction between place and silent cells starting from the very beginning of map formation.

RESULTS

We obtained whole-cell current-clamp recordings of dorsal hippocampal CA1 pyramidal neurons as rats moved around a previously unexplored “O”-shaped arena (for 7.9 ± 2.3 min). Nine rats went around the maze a sufficient number of times in the same direction (clockwise, CW, or counterclockwise, CCW) to allow determination of whether the recorded neuron was a place (PC, $n = 4$) or silent (SC, $n = 5$) cell in that environment based on its spiking (see Experimental Procedures). In three cases, both directions qualified. Since cells in one-dimensional mazes often have different place fields in each direction, including cases with a place field in one but not the other direction, this gave 12 directions (4.9 ± 0.9 laps each) to classify as having place fields (PD, $n = 5$) or being silent (SD, $n = 7$). These numbers agree with the extracellularly-determined fraction of place cells in a given environment (Thompson and Best, 1989; Wilson and McNaughton, 1993; Karlsson and Frank, 2008), suggesting that extracellular methods can accurately sample silent cells.

Figure 2 shows an intracellularly recorded place cell that fired in one corner of the maze (Figures 2A and 2B) and had place fields at that location in both directions (Figure 2C). The AP firing rate map for all periods when the animal faced the CCW direction

is shown in original (Figure 2B) and linearized (Figure 2D; Experimental Procedures) coordinates. A 3 min V_m trace during 3 successive CCW laps (Figure 2E) shows that each pass through the place field was accompanied by high AP firing rates as well as a clear subthreshold depolarization under that spiking (A.K. Lee et al., 2008, Soc. Neurosci., abstract [690.22]; Harvey et al., 2009). The sustained nature of these depolarizations suggests that spatially tuned spiking is not simply due to a short timescale coincidence detection mechanism. Some (Figure 2E, trace 1), but not all (trace 2), passes revealed spiking associated with a series of large (to ~ -25 mV), long-lasting (~ 100 ms) depolarizations (Kandel and Spencer, 1961; Wong and Prince, 1978; Traub and Llinás, 1979; Takahashi and Magee, 2009) occurring rhythmically at $\sim 4\text{--}5$ Hz (theta frequency).

Figure 3 shows an intracellularly recorded silent cell that fired very few spikes in the maze and did not have a place field in either direction (Figures 3A–3D). CCW direction spiking occurred mostly during 1 lap (Figure 3C) and thus did not satisfy the consistency criterion for place fields (Experimental Procedures). An ~ 3 min trace shows that the V_m was very flat as the animal moved around the maze (here ~ 1.5 CW laps) (Figure 3E). An expanded trace (Figure 3E, above right) reveals ~ 5 Hz, $\sim 5\text{--}10$ mV subthreshold fluctuations.

We estimated the net input into the cell as seen at the soma as a function of the animal's location. This was done for each direction of each cell as follows. We first removed all APs and any parts of the V_m trace directly attributable to the spikes themselves, i.e., parts representing spike-associated regenerative and/or other intrinsic processes at the soma as distinct from the inputs that triggered the spikes (see Figures S1A–S1C available online; Experimental Procedures). This included removing (1) spike after-depolarizations (ADPs), which can be >5 mV and last for >20 ms for single APs and can accumulate for successive APs (Figures S1A and S1B; Kandel and Spencer, 1961; Wong and Prince, 1978; Traub and Llinás, 1979; Jensen et al., 1996), and (2) the entirety of the slow, large, putatively calcium-based depolarizations that often follow a burst of APs, which can

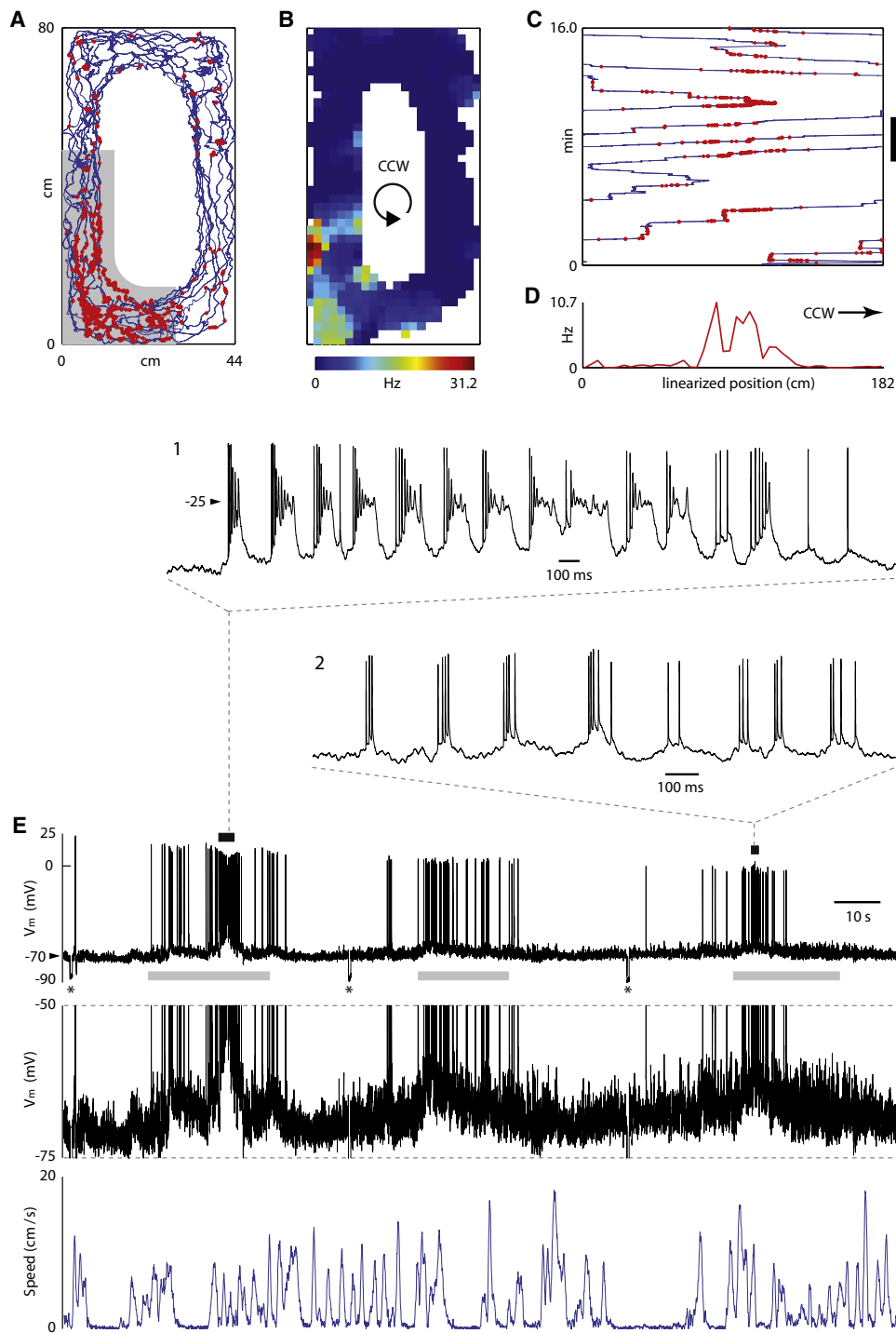


Figure 2. Whole-Cell Recording of a Hippocampal CA1 Place Cell in a Freely Moving Rat Exploring a Novel Maze

(A) Trajectory of animal (blue) and locations where APs occurred (red) during entire 16 min awake recording in "O"-shaped maze (inner wall not shown).

(B) AP firing rate map during periods when animal faced CCW direction.

(C) Linearized location (measured around oval maze path) of animal (blue) and APs (red) as a function of time.

(D) Linearized AP firing rate map for CCW direction.

(E) V_m (black, lowest trace expands trace above it around narrower V_m range) and head speed (blue) during three successive CCW laps (corresponding to black vertical bar in C). Gray bars correspond to shaded place field region in (A). Above: two passes through the place field. *'s mark brief hyperpolarizing current steps used to probe R_N and membrane time constant (τ_m).

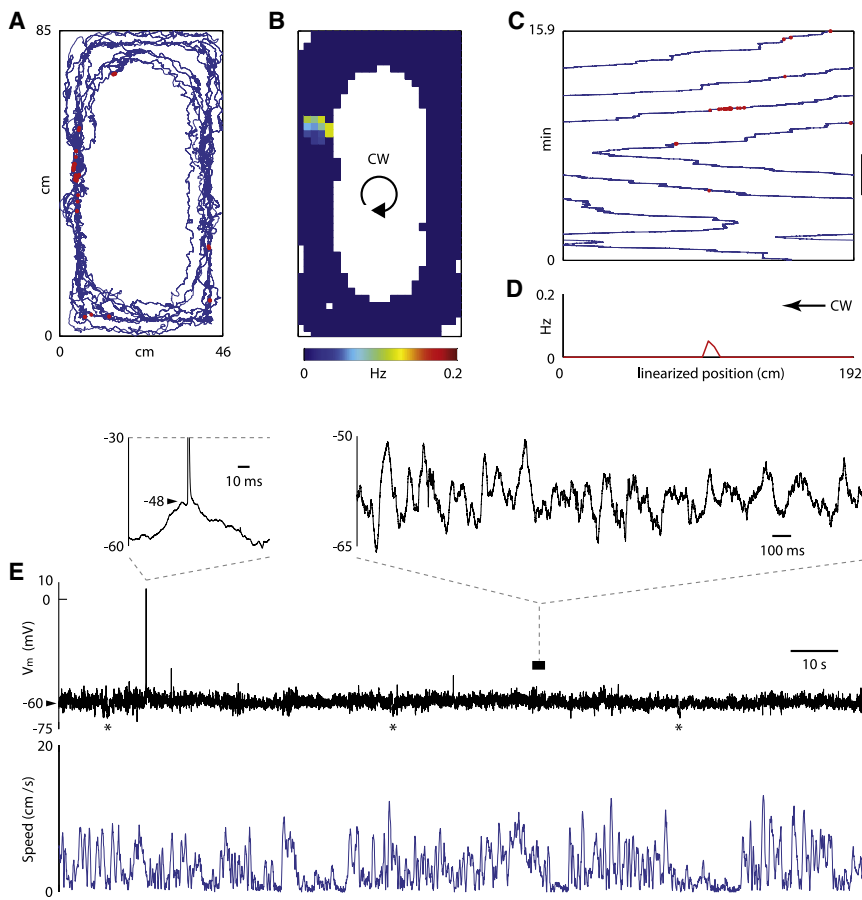


Figure 3. Whole-Cell Recording of a Hippocampal CA1 Silent Cell in a Freely Moving Rat Exploring a Novel Maze

(A) Trajectory of animal (blue) and locations where APs occurred (red) during entire 16 min awake recording.
 (B) AP firing rate map during periods when animal faced CW direction.
 (C) Linearized location of animal (blue) and APs (red) as a function of time.
 (D) Linearized AP firing rate map for CW direction.
 (E) V_m (black) and head speed (blue) during ~1.5 CW laps (corresponding to black vertical bar in C). Above: V_m dynamics leading to AP (left), V_m theta frequency oscillations (right).

be >25 mV and last for >50 ms (Figure S1C; Kandel and Spencer, 1961; Wong and Prince, 1978; Traub and Llinás, 1979). Then the remaining V_m trace was linearly interpolated across the gaps (Figures S1A–S1C) and the mean of the resulting trace as a function of location computed (Figure 4A, black). While the classical, i.e., mean spiking rate, place field (Figure 4A, red) represents the output of the cell, this mean “subthreshold field” reflects the spatially-modulated, net input into the cell’s soma.

We determined the AP threshold of each cell as follows. The threshold for individual APs varies, especially (1) within a burst, rising with successive APs (Figure S1B; Kandel and Spencer, 1961), (2) during longer periods of depolarized V_m (e.g., within the place field), where it is elevated (Figure S1D; Azouz and Gray, 2003). Because we wanted the threshold to truly represent a threshold in the sense of the minimum V_m required to trigger APs and wanted a single such value for each cell, we set it to be the mean threshold of isolated APs and first APs of bursts occurring during less-depolarized periods (Figures S1D and S1E; Experimental Procedures). Note that this is why the subthreshold field could go above the threshold so determined (Figure 4A).

Analysis of the mean subthreshold fields and intrinsic parameters revealed both similarities and striking differences between place field (PD) and silent (SD) directions and between place (PC) and silent (SC) cells (Figures 4A–4G and S1F–S1L). One might

suppose place fields resulted from a higher baseline V_m , making spiking more likely given similar depolarization by inputs (Figures 1A versus 1B), but their baselines were on average more hyperpolarized than those of silent directions, though the difference did not reach statistical significance (-65.5 ± 2.2 versus -59.2 ± 1.8 mV; $p = 0.059$) (Figure 4B). Perhaps place fields had a higher peak V_m , irrespective of baseline levels (e.g., Figures 1A versus 1B or 1C)? Yes (-52.7 ± 2.0 versus -56.3 ± 1.7 mV; $p = 0.20$), but the values for both classes largely overlapped and thus could not alone determine which directions would have place fields (Figure 4C). Or perhaps

place field baseline-to-threshold distances were smaller, independent of absolute baseline or threshold values, again making spiking more likely given similar input-based depolarizations (e.g., Figures 1A versus 1B or 1D)? While slightly smaller on average (9.7 ± 1.6 versus 11.9 ± 0.6 mV; $p = 0.24$), again the classes overlapped substantially (Figure 4D).

A clear possibility is that place cells have larger input-based depolarizations than silent cells. This was indeed the case. For place fields, the mean subthreshold field displayed an ~5–20 mV (12.8 ± 2.8 mV) (Figure 4E) hill-shaped depolarization above the baseline that generally closely followed the shape of the AP firing rate field (Figure 4A; A.K. Lee et al., 2008, Soc. Neurosci., abstract [690.22]; Harvey et al., 2009). The roughly unimodal nature of these subthreshold fields suggests that spatially tuned spiking does not simply result from thresholding spatially random inputs but instead that the net input is itself already spatially tuned. Silent directions, in contrast, had strikingly flat subthreshold fields (“peak – baseline” = 12.8 ± 2.8 mV [place] versus 2.9 ± 0.3 mV [silent], $p = 0.024$) (Figures 4A and 4E). The somatic input resistance (R_N) (Supplemental Experimental Procedures), which can be considered an intrinsic property in some cases and input-dependent in others, was not larger for place cells (Figure S1K), thus the larger “peak – baseline” of place fields did not result from a higher R_N , which could have magnified the effect of inputs on V_m level. Together, these

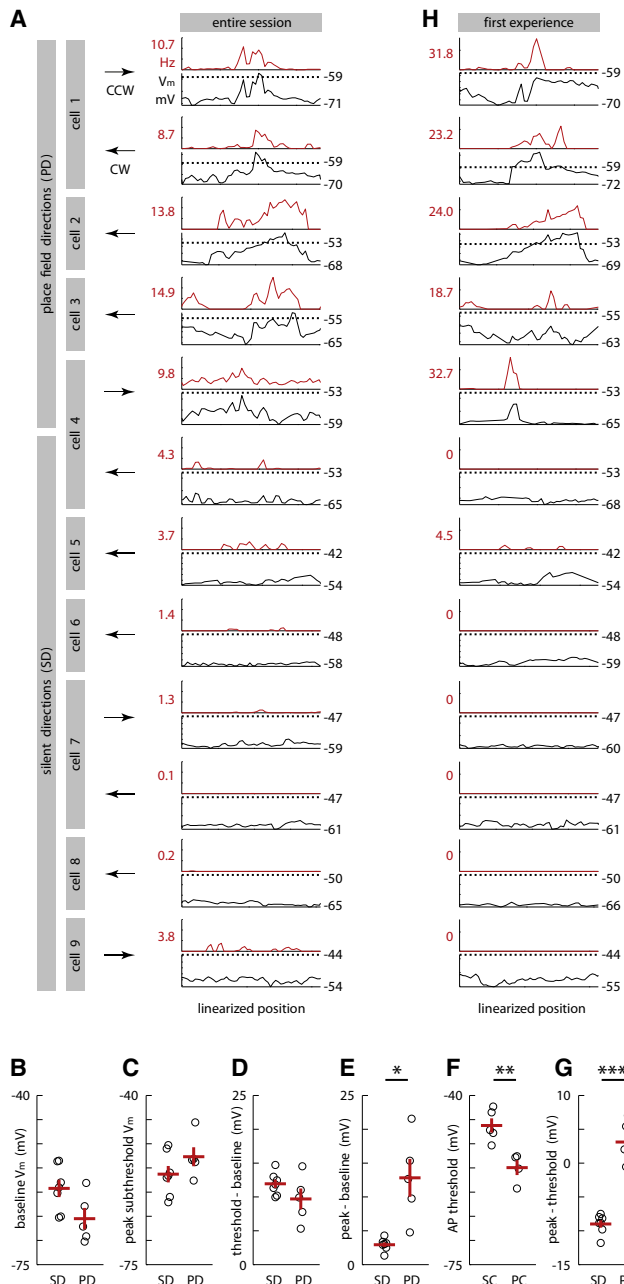


Figure 4. Classical Spiking Place Fields and Subthreshold Fields of Hippocampal Place and Silent Cells in a Novel Environment

(A) Mean AP rate (red) and mean subthreshold V_m (black) as a function of animal location, averaged over all periods in that direction. AP plots: uniform 0–15 Hz scale, peak rate (left). Subthreshold plots: individual scales, AP threshold (dotted), minimum V_m (bottom).

(B–G) Intracellular features of place versus silent cells or directions (mean \pm SEM, red). Horizontal jitter added to individual values for visibility. Place cells (PC): cells 1–4; silent cells (SC): 5–9. PD = place field directions, SD = silent directions. **, *** correspond to $p < 0.05, 0.005, 0.0005$ differences. See text.

See also Figure S1.

peaked and flat subthreshold field shapes suggest a sparse or highly non-random distribution of inputs.

The difference in “peak – baseline” values could alone explain place field spiking versus silence as their respective distributions did not overlap (Figure 4E); however, the AP threshold was also clearly lower for place than silent cells (-54.9 ± 1.5 versus -46.2 ± 1.5 mV; $p = 0.0049$) and thus could itself account for the difference between the two classes (Figure 4F). Therefore, unexpectedly, input-based or intrinsic features could each underlie which cells become place or silent cells. The surprising correlation between these features (“peak – baseline” and threshold) could also be seen directly ($\rho = -0.67$; $p = 0.018$) (Figure S1O). Furthermore, as was true for individual APs within a cell (Figure S1D), the threshold was correlated with the baseline V_m across cells ($\rho = 0.88$; $p = 0.00013$) (Figure S1P).

The largest underlying difference we found between place field and silent directions was the relationship between their peak subthreshold V_m values and corresponding thresholds. The peak got near to or crossed above threshold for place fields but generally remained far below threshold for silent directions (Figures 4A and 4G). This “peak – threshold” difference was the most statistically significant feature separating the two classes (place: 3.1 ± 1.4 mV versus silent: -9.0 ± 0.5 mV, $p = 0.00033$), with an unexpected and visibly large gap (of 6.5 mV) between them (Figure 4G). While, by definition, the “peak – threshold” would be expected to be higher for place field directions, there was no reason to assume the presence of any gap at all, much less one this wide.

An additional nine recordings (duration 4.2 ± 1.7 min) in which animals sampled the maze ≤ 1 time were similarly analyzed. The reduced sampling prevented definitive classification into place field or silent directions, but these cells could be clearly categorized as active ($n = 7$) or nonactive ($n = 2$) based on overall firing rates, then were grouped with the place and silent cells into active (AC, $n = 11$) or nonactive (NC, $n = 7$) cell and active (AD, $n = 12$) or nonactive (ND, $n = 9$) direction classes (Experimental Procedures). The main results were confirmed in this expanded data set (Figures S1Q–S1G'). Active cells had peaked versus flat subthreshold fields (“peak – baseline” = 11.5 ± 1.6 mV [active] versus 3.2 ± 0.5 mV [nonactive], $p = 0.00032$) (Figure S1T) and lower AP thresholds (-53.6 ± 1.5 versus -46.2 ± 1.5 mV, $p = 0.0049$) (Figure S1U), while the baseline V_m values of active and nonactive directions largely overlapped (Figure S1Q). Again the “peak – baseline” and threshold were negatively correlated ($\rho = -0.47$; $p = 0.050$) (Figure S1F') and the threshold and baseline positively correlated ($\rho = 0.81$; $p = 0.000039$) (Figure S1G') across cells. Unlike before, the differences in peak subthreshold V_m (Figure S1R) and “threshold – baseline” (Figure S1S) reached statistical significance, though the distributions still largely overlapped, and there was some overlap in the “peak – baseline” (Figure S1T) and threshold (Figure S1U) distributions. However, as before, the “peak – threshold” difference was the most statistically significant separating feature (active: 2.7 ± 0.8 mV versus nonactive: -8.7 ± 0.5 mV, $p = 3.3 \times 10^{-9}$), again with a bimodal distribution and large gap (of 5.5 mV) between the two classes (Figure S1V). Indeed, the “peak – threshold” value was the only feature clearly separating active and nonactive directions (besides the overall

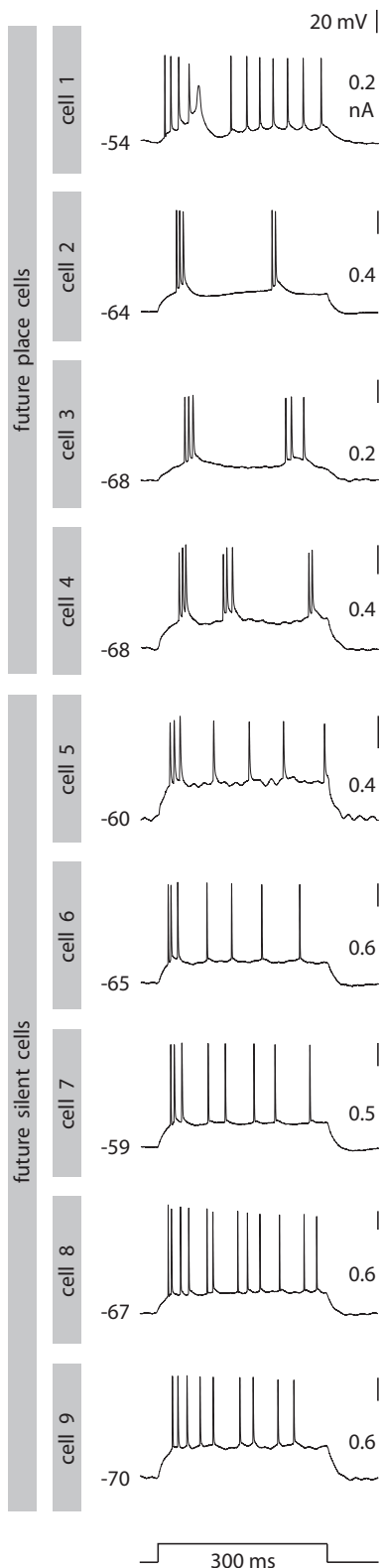


Figure 5. Pre-exploration Firing Pattern in Response to Depolarizing Current Injection for Each Eventual Place and Silent Cell in Figure 4A
Current step amplitude (right).

AP rate, which was used to define the classes in the first place) (Figures S1Q–S1E'). Overall, both the place field and silent direction as well as active and nonactive direction results support the picture of silent cells shown in Figure 1E.

The hippocampal CA1 spatial map is thought to form in the first few minutes when exploring a novel environment (Hill, 1978; Wilson and McNaughton, 1993; Frank et al., 2004; Leutgeb et al., 2004). Here, during the first experience of each location in each direction, place cells had spatially selective firing in the same locations as during the entire session, and the subthreshold fields generally also followed this pattern (Figure 4H). Moreover, silent directions were silent during the initial experience and their subthreshold fields were also essentially flat and far below threshold from the beginning (Figure 4H). This subthreshold result agrees with extracellular studies showing that ~80% of spiking place fields were present upon first experience of a given maze (Hill, 1978; Frank et al., 2004) and shows that spatial selectivity of both CA1 pyramidal cell inputs and outputs was present by the first exposure to a novel environment. Also, thresholds of the first AP during exploration were lower for place than silent cells (-54.0 ± 0.8 versus -44.5 ± 3.3 mV, $p = 0.041$), as was the case for the entire session (Figure 4F).

Going back yet earlier in time, we investigated cellular responses to current steps in the anesthetized animal before any spatial experience with the maze to see whether intrinsic properties of place and silent cells differed a priori (Experimental Procedures). Most unexpectedly, future place cells exhibited far more bursting to depolarizing current steps than silent cells (fraction of APs in bursts = 0.80 ± 0.15 versus 0.24 ± 0.02 , $p = 0.033$) (Figures 5 and S1J). Other pre-exploration intrinsic parameters, including the pre-exploration AP threshold, did not significantly differ (Figures S1F–S1I), though the pre-exploration and awake thresholds were correlated ($\rho = 0.71$; $p = 0.034$), suggesting initial traces of the later difference. The difference in pre-exploration burst propensity and lack thereof with respect to other features also held for the expanded set of active and nonactive cells (fraction of APs in bursts = 0.62 ± 0.09 versus 0.20 ± 0.04 , $p = 0.00092$) (Figures S1W–S1A').

A prominent feature of our recordings was the presence during behavior of “complex-spike” (CS) events consisting of ≥ 1 AP(s) followed by a large, long-lasting depolarization (Figure 2E, trace 1; Kandel and Spencer, 1961; Wong and Prince, 1978; Traub and Llinás, 1979; Harvey et al., 2009; Takahashi and Magee, 2009). From *in vitro* studies, such events are believed to require strong or synchronous input (Takahashi and Magee, 2009). Importantly, these substantial, calcium-mediated (Wong and Prince, 1978; Traub and Llinás, 1979) depolarizations could trigger various plasticity mechanisms (Sjöström and Nelson, 2002). We classified events as CSs by analyzing the slow depolarization after fast APs were removed (Figure 6A, left; Experimental Procedures). Figure 6A shows similar CS shapes from two neurons, while Figure 6B shows the variety of “complex” shapes these events could take. The slow depolarizations plateaued around -25 mV (Figure S2A; Experimental Procedures). Though somatic APs appear blocked during these depolarizations, axonal APs may continue to be triggered (Mathy et al., 2009). Occasionally, even longer depolarizations occurred (Figure 6B,

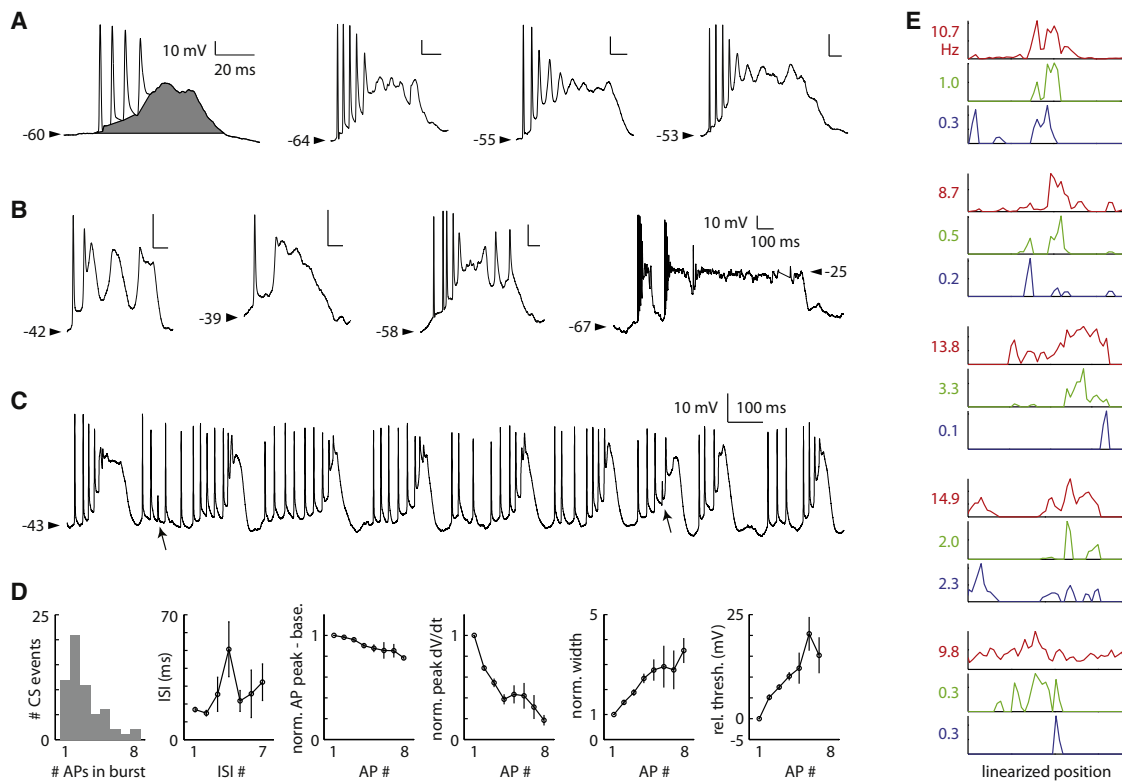


Figure 6. Complex-Spike (CS) Events at the Soma of CA1 Pyramidal Cells in Freely Moving Rats Exploring a Novel Maze

- (A) Examples of similarly-shaped CSs from two cells. Shaded area marks large, slow depolarization used in CS classification (left).
- (B) Examples of CS shape variety from same two cells in (A). “Plateau-like” event occurring within place field (right).
- (C) Series of CSs occurring within a place field. Arrows mark spikelets, and 55.7% of APs in this trace had shoulders (i.e., were immediately preceded by spikelet-like events).
- (D) Statistics of APs within CSs for Figure 2 place cell (mean \pm SEM). No “relative threshold” value for AP #8 (right) because all were shoulder APs (Experimental Procedures).
- (E) AP (red), CS (green), and extracellularly defined complex spike (blue) rates as a function of animal position for Figure 4A place fields. Peak rates (left). See also Figure S2.

right), some resembling “plateau potentials” described previously *in vitro* (Fraser and MacVICAR, 1996; Suzuki et al., 2008). Neurons sometimes fired series of CSs rhythmically at \sim 4–5 Hz (Figures S2B and S2C) within the place field (Figures 2E, trace 1, and 6C), as can be elicited by a large, constant inward current (Kamondi et al., 1998). CS APs had long inter-spike intervals (ISIs), decreasing peak values of the rising slope, dV/dt (first derivative of V_m with respect to time), and increasing width and threshold (Figure 6D; Kandel and Spencer, 1961). In comparison, extracellularly recorded “complex spikes” are defined by significantly shorter ISIs (1.5–6 ms) (Ranck, 1973). Just 5.0% of our intracellularly-classified CSs contained at least one ISI \leq 6 ms, thus intracellular recording may be required to detect these special, possibly plasticity-inducing events.

CSs occurred much more frequently for place field than silent directions (0.20 ± 0.14 versus 0.0011 ± 0.0007 Hz; $p = 0.0025$) (Figure S1N), containing 12.6% (23.2%) of all APs and occurring in 66.7% (6.3%) of all laps in place field (silent) directions. Furthermore, CSs (Figure 6E, green) were concentrated at the centers of standard AP place fields (Figure 6E, red), while events that would have been classified as “complex spikes” using

extracellular recordings fired off-center (Figure 6E, blue; Harris et al., 2001). CSs therefore carry a strong spatial signal.

DISCUSSION

The subthreshold field, AP threshold, and CSs reveal previously hidden, but likely crucial, variables for forming spatial maps and possibly memories of specific items and events. Previous intracellular recordings have shown that a sustained subthreshold depolarizing hill underlies the region of place field spiking in both freely moving rats (A.K. Lee et al., 2008, Soc. Neurosci., abstract [690.22]) and head-fixed mice navigating a virtual reality environment (Harvey et al., 2009) and that spikelets (J. Epsztain et al., 2008, Soc. Neurosci., abstract [690.21]) can strongly influence spatial firing (Epsztain et al., 2010). Here, for the first time, we measured the input-based subthreshold field of silent cells as well as fundamental intrinsic properties of both place and silent cells, revealing the interaction of inputs and cellular features underlying place and silent cell determination in an environment. Furthermore, to capture the beginning of spatial memory formation, our measurements were made in animals exploring the

environment for the first time, as opposed to those running in familiar mazes (Harvey et al., 2009). Also, while the existence of intracellular CSs in place cells has been noted before (Harvey et al., 2009), here we characterized CSs as individual events (Figures 6A, 6B, 6D, and S2A), as events that often fired rhythmically at theta frequencies (Figures 2E, trace 1, 6C, S2B, and S2C), and in terms of their spatial firing patterns (Figure 6E). Moreover, we showed that they differ from extracellularly classified CSs. In particular, intracellular CSs, unlike extracellular ones, are tuned to place field centers (Figure 6E). Regarding methods, our anesthesia + wakeup protocol yielded basic data in agreement with methods not involving such a procedure: place fields like those recorded extracellularly, subthreshold fields of place cells similar in shape to those from other intracellular experiments (Harvey et al., 2009), and place and silent cell proportions comparable to extracellular values (Thompson and Best, 1989; Wilson and McNaughton, 1993; Karlsson and Frank, 2008).

A basic hypothesis for the origin of place fields would be that a multitude of (excitatory as well as inhibitory) inputs randomly summate to produce depolarizing hills of differing amplitudes in different cells, and these then interact with a fixed AP threshold such that larger hills yield place cells and smaller ones silent cells. Consistent with this, the subthreshold field “peak – baseline” of place fields was in each case larger than that of silent directions (Figure 4E).

However, several other results imply a more structured process for selecting which cells will have place fields in a novel environment than this random input-based model. First, place cells had clearly lower thresholds than silent cells (Figures 4F and S1E), including from the start of exploration. This suggests a critical role for intrinsic properties in determining which cells become place or silent cells. While we cannot rule out some effect of nonintrinsic factors (e.g., inputs) on our measure of the awake threshold since it was based on spontaneous APs, the correlation between this threshold and the pre-exploration one using experimenter-evoked APs supports an intrinsic origin of the awake value. What could underlie such a difference in thresholds? The correlation between the threshold and baseline V_m (Figures S1D, S1P, and S1G') suggests that the former could be set by the latter. Also, cholinergic modulation can change thresholds by several millivolts even with a constant baseline (Figenschou et al., 1996). Alternatively, having a higher proportion of APs triggered by dendritic spikes (Gasparini et al., 2004) could lead to an apparently lower threshold, with the proportion itself affected by differences in inputs and/or intrinsic factors.

Second, while the random input-based model predicts a continuum of “peak – threshold” values (regardless of whether the AP threshold is fixed or varies across cells) with higher values for place cells, instead we found a bimodal distribution with a large, clear gap separating place fields from silent (Figure 4G) as well as active from nonactive (Figure S1V) directions. This was the feature that most clearly separated the two classes and, contrary to the random input-based model, suggests that place and silent cells qualitatively differ within a given environment. This qualitative difference is further supported by the surprising flatness of the silent cells’ subthreshold fields (Figures 4A, 4E, and 4H). A nonrandom distribution of inputs could explain the

lack of a continuum, but would be unlikely to explain the following result, as it involved somatic current injection.

Third, even prior to any sensory input from the maze, future place and silent cells unexpectedly displayed differing burst propensities (Figures 5 and S1J) as did future active and non-active cells (Figure S1A'). Thus intrinsic properties may predetermine the division into place and silent cells. Does this mean that a fixed fraction of cells will have place fields regardless of the size of the environment? While fewer cells may express place fields in smaller and/or simpler mazes (Thompson and Best, 1989), in larger environments the number of place cells appears to be limited, with additional spatial coverage achieved primarily by having each place cell express multiple fields (Fenton et al., 2008; Davidson et al., 2009). Therefore, what intrinsic factors may predetermine is the restricted subset of cells that could potentially have place fields. Moreover, among the set of possible place cells, the relative locations of their place fields also appear to be predetermined (Dragoi and Tonegawa, 2011).

In the simple input-based model, the subthreshold field would essentially reflect the net synaptic conductance as a function of the animal’s location and be largely independent of properties such as the threshold or burst propensity, but these results show that they are all interrelated. Indeed, direct comparison of the “peak – baseline” and threshold shows that these features were negatively correlated (Figures S1O and S1F') as opposed to uncorrelated (or positively correlated, which could occur if the input and threshold were uncorrelated but the threshold acted as a ceiling on the subthreshold peak). Instead, our results imply that the subthreshold field itself may be strongly shaped by the same intrinsic factors underlying the threshold and bursting. For instance, a subset of neurons, i.e., those that become place cells, could possess dendritic segments with greater excitability (Frick et al., 2004; Losonczy et al., 2008), organized such that a spatially uniform set of synaptic inputs is converted into a spatially tuned input as seen by the soma (Jia et al., 2010).

These results should therefore lead to new classes of models (O’Keefe and Burgess, 2005; McNaughton et al., 2006; Solstad et al., 2006; de Almeida et al., 2009) of place field formation based on grid cell (Hafting et al., 2005) or other inputs as well as models of memory formation in general. Specifically, a role for intrinsic parameters should be added to that of external (e.g., sensory-driven) input.

If intrinsic features are critical for selecting which cells become place cells, how do different environments become represented by different subsets of place cells (O’Keefe and Conway, 1978; Muller and Kubie, 1987; Thompson and Best, 1989; Leutgeb et al., 2005)? In such a “global remapping,” many cells silent in one maze have place fields in another. Furthermore, ~20% of eventual place cells in a given novel environment are initially silent there (Hill, 1978; Frank et al., 2004). Thus, the selection factors cannot be permanently associated with each neuron. Instead, they may be randomized after a new map has been learned so that the next novel maze can be encoded by a statistically independent subset of place cells (Leutgeb et al., 2005). For this, the ability to alter burst propensity (Staff et al., 2000; Moore et al., 2009), the threshold (Figenschou et al., 1996), dendritic excitability (Frick et al., 2004; Losonczy et al., 2008),

or other forms of excitability (Oh et al., 2003) could be especially relevant (Zhang and Linden, 2003). However, it is still possible that a subset of neurons is silent in all environments (Thompson and Best, 1989).

Lastly, what role do CSs play? Across repeated sessions in a given environment, the map is consistent (Thompson and Best, 1990), even with intervening sessions in other mazes (Leutgeb et al., 2005). But if the intrinsic features critical for place cell determination change, how is the correct map recalled when the animal encounters a familiar versus novel environment? The specific location of each place field appears to be determined very early during exploration of a novel maze (Figures 4A and 4H), and plasticity induced by the rhythmically occurring (Figures 2E, trace 1, 6C, S2B, and S2C), spatially tuned (Figure 6E) CSs may then refine (McHugh et al., 1996; Frank et al., 2004; Karlsson and Frank, 2008) and stabilize (Kentros et al., 1998) that map for long-term storage—a process that should include converting the intrinsically based firing in a novel environment into synaptic-based firing as the environment becomes familiar. Without such a conversion, a new map would appear for each experience in the same maze, as seen when plasticity has been blocked (Kentros et al., 1998). With a conversion to input-based firing, when an animal encounters a familiar instead of novel environment, the map stored in memory can override any current internal settings ready to express a new set of place cells for encoding new spatial memories.

EXPERIMENTAL PROCEDURES

Surgery, Electrophysiology, and Behavior

The recording method has been previously described in detail (Lee et al., 2006, 2009). Briefly, head-anchored whole-cell recordings in freely moving animals were obtained in experimentally naive P24–27 male Wistar rats. Animals were anesthetized with medetomidine (225 µg/kg), midazolam (6 mg/kg), and fentanyl (7.5 µg/kg), then head-fixed into a stereotaxic frame. A craniotomy was made 3.5 mm posterior of bregma, 2.5 mm lateral of midline over the right hemisphere. Blind *in vivo* whole-cell recordings were obtained in the dorsal CA1 region of the hippocampus (Margrie et al., 2002; Lee et al., 2009). Pipettes (5–7 MΩ) were filled with an intracellular solution containing (in mM) K-gluconate 135, HEPES 10, Na₂-phosphocreatine 10, KCl 4, MgATP 4, and Na₃GTP 0.3 (pH adjusted to 7.2) as well as biocytin (~0.05%). After obtaining a whole-cell recording, dental acrylic was applied to anchor the pipette rigidly with respect to the skull. After the acrylic hardened, the animal was moved from the stereotaxic frame to an “O”-shaped arena (outer dimensions ~45 × 80 cm, ~20 cm high inner and outer walls, ~10 cm wide path between inner and outer walls). Then the anesthetic mixture was antagonized with atipamezole (1 mg/kg), flumazenil (600 µg/kg), and naloxone (180 µg/kg). After ~1–3 min the animal woke, then explored the arena for the first time. When exploration stopped, the experimenter encouraged the animal to continue moving around the maze by gently lifting its tail or touching its back. Current-clamp measurements of V_m were sampled at 20 kHz while the animal's behavior in the maze was captured on video and its location tracked at 25 Hz. For nine cells, the animal sampled each location in the maze while facing a given direction (CW or CCW) ≥2 times (with 1 exception; see the “Place Field Classification” section). These recordings were used for place and silent cell analysis. For four of these cells, a small hyperpolarizing holding current (−0.020 to −0.135 nA) was applied. Recordings were corrected offline for nonzero current across the series resistance. Recordings were not corrected for the liquid junction potential. At the end of recording, the animal was given an overdose of ketamine and perfused with 0.1 M phosphate-buffered saline followed by a 4% paraformaldehyde solution. Neurons were visualized with the avidin-biotin peroxidase method. All nine neurons

had the depth and electrophysiological characteristics of somatic CA1 pyramidal cell recordings, and six of these cells were histologically verified to be CA1 pyramidal cells (with no evidence of non-CA1-pyramidal-cell filling in the other three animals). An additional nine recordings, in which the animal sampled each location in the maze in a given direction ≤1 time, were included with the original nine cells for active and nonactive cell analysis (Figures S1Q–S1G'). For five of these cells, hyperpolarizing holding current was applied (−0.009 to −0.040 nA), and for one cell the holding current was not recorded. Four of these recordings were histologically verified to be from CA1 pyramidal cells. Most of the eighteen recordings were used in a previous study (Epsztain et al., 2010). All procedures were performed according to German guidelines on animal welfare.

Data Analysis

All analysis was done using custom-written programs in Matlab. All values are reported as mean ± SEM unless otherwise noted. All place versus silent and active versus nonactive comparisons were done using the unpaired t test assuming unequal variances unless otherwise noted, in which case the nonparametric Mann-Whitney *U* test was used. Pearson's linear correlation coefficient was used to assess correlations (ρ) between features, with significance determined with respect to the hypothesis that there was no correlation. All p values reported are two sided.

Place Field Classification

The following procedure (Epsztain et al., 2010) was used to determine whether a cell has a place field in a given direction. Only directions in which the animal sampled each location in ≥2 different laps were considered. The locations in the maze were collapsed onto an ~2 m long curve that went around the “O”-shaped track, giving a one-dimensional representation of animal location. The beginning (position 0) and end of this curve were arbitrary and identified as the same location, preserving the maze's cyclical structure. The curve was divided into 4 cm wide segments. Only time periods when the animal's head faced within 75 degrees of the given direction (CW or CCW) were considered. The AP firing rate as a function of the animal's one-dimensional location in the given direction (Figures 2D, 3D, 4A, and 6E, red) was computed as the number of APs that occurred when the head of the animal was within a given pair of adjacent segments divided by the total amount of time the animal's head was there, and this rate was assigned to the location at the middle of the segment pair. Thus the rate was computed every 4 cm with 8 cm wide boxcar smoothing. If the total duration that the head was within a pair of segments was <0.2 s, no rate was assigned to that location. Then (1) the baseline firing rate was set as the mean rate of the 10% of lowest rate positions, (2) the position of the peak rate was determined, (3) the full session candidate (place) field around the peak was determined by adding any contiguous positions (called the “inside” of the field) where the rate was ≥ the baseline rate plus 20% of the difference between the peak and baseline rates, and (4) the peak rate outside of the candidate field was also determined. Steps 1–3 were then repeated for each individual lap separately, thus producing fields for individual laps too. To classify a direction as having a place field, (1) the full session candidate field had to be ≥12 cm (i.e., 3 positions) wide, (2) the full session's highest peak outside the full session field had to be ≤ the baseline rate plus 2/3 of the difference between the full session peak and baseline rates (i.e., unimodality), and (3) ≥2/3 of the individual laps had to have fields that overlapped the full session field (i.e., consistency). A direction satisfying these conditions was classified as having a place field (PD). Few APs were fired in directions that did not have a place field so defined (Figure S1M), so all those directions were classified as silent (SD). A place cell (PC) is a cell with a place field in at least one direction; otherwise, it was classified as a silent cell (SC) even if only one direction could be analyzed. There were two special cases. For cell 3 (Figure 4A), the animal completed ~1.5 instead of ≥2 CW laps, however it passed through the full session candidate field twice and both times the individual lap fields were aligned, so we classified it as a place field. For the CCW direction of cell 4 (Figure 4A), the full session place field was determined starting with the seventh CCW lap and continuing through the last CCW lap. This is because the individual lap fields shifted location in the first six laps (as can happen in novel environments for a subset of cells) but had a consistent location starting in the seventh lap onward. Interestingly, the firing during the

first experience with each position in the CCW direction (Figure 4H) was located in the same place as the eventual place field from the seventh lap on.

Active versus Nonactive Cell Classification

The AP firing rates of the 5 place field and 7 silent directions were distributed such that all place field direction rates were >1.46 Hz and all silent direction rates were <1.02 Hz; thus, the place field directions were also classified as “active” and silent directions as “nonactive.” The four place cells were also classified as “active” and the five silent cells as “nonactive.” These firing rates were then used to classify the nine directions of the nine additional cells (1 direction per cell) into seven active directions, all of which had rates >1.54 Hz, and two nonactive directions, both of which had rates <0.020 Hz. Together, this yielded 12 active and 9 nonactive directions, and 11 active and 7 nonactive cells.

Determination of AP Threshold

The principles used for determining the awake AP threshold were (1) the threshold should truly represent a threshold in the sense of the minimum V_m required to trigger an AP, and (2) there should be a single such value for each cell. For each AP, we set the threshold to be the V_m value at which the dV/dt crossed 10 V/s (or $0.33 \times$ the peak dV/dt of that AP, whichever was lower, in order to handle the slower APs that occurred later within bursts and CSs) on its way to the AP peak V_m . Across all APs of a given cell, the threshold of individual APs varied, particularly during (1) a burst with short ISIs or a CS, where successive APs had higher thresholds, and (2) a longer period of depolarized V_m (e.g., within the place field), where the threshold was elevated. Because these cases involved conditions without a steady baseline V_m , we determined the cell’s threshold after excluding all APs except isolated APs and the first APs in bursts defined based on ISIs alone (with the maximum ISI conservatively set to 50 ms, meaning that an AP needed to not have another AP occurring within 50 ms before it), as well as excluding all APs (including the first AP) in CSs. We also excluded APs with shoulders (Epsztein et al., 2010), as such spikelet-AP events could be triggered from different V_m levels than full-blown APs. To exclude APs during longer periods of depolarized V_m , for each remaining AP we computed the mean of the immediately preceding subthreshold V_m level from 1000 ms before to 50 ms before the AP peak (using the interpolated subthreshold V_m trace described in the “Determination of Subthreshold Field” section), then plotted the threshold as a function of this preceding subthreshold level (Figure S1D). This shows that the threshold was indeed higher for APs triggered from more depolarized levels. To select a single but robust minimum value for the threshold of each cell, we determined the 2.5% (Figure S1D (a)) to 97.5% (Figure S1D (b)) range of preceding subthreshold levels, selected the APs between the 2.5% line and the line (Figure S1D (c)) 20% of the way from the 2.5% to 97.5% line, then took the mean threshold of those APs. That is, we selected a subset of APs that occurred during less-depolarized periods for determining the threshold. In practice, 10 V/s appeared best for detecting when an individual AP started to “take off” (Figure S1E). But we also used an alternative method for determining the threshold of individual APs: setting the dV/dt threshold to be 10% of that AP’s peak dV/dt . This did not change the result that the threshold of place cells was much lower than that of silent cells (-55.2 ± 1.4 versus -45.8 ± 1.2 mV; $p = 0.0019$). For determining the threshold of the first AP, we followed the same exclusion procedure as described above except we did not exclude APs based on the preceding subthreshold V_m level, then we took the 10 V/s threshold of the earliest remaining AP. For determining the pre-exploration AP threshold (during anesthesia) for each cell, we averaged the 10 V/s-based thresholds of the first APs that were rapidly triggered by depolarizing current steps applied immediately upon breaking into the neuron and achieving the whole-cell recording configuration. An exception was made for cell 1, which fired some spontaneous APs at that time; thus, threshold was determined from the 10 V/s-based thresholds of those APs.

Determination of Subthreshold Field

To compute the mean somatic subthreshold V_m as a function of the animal’s location for a given head direction (CW or CCW) (Figure 4A, black), we developed a method for estimating the somatic subthreshold V_m trace by removing all APs and any parts of the trace directly attributable to the somatic spikes

themselves (Figures S1A–S1C). The parts to remove included the ADP after each individual AP (Figure S1A, left), the accumulated ADPs for successive APs of a burst (observing that for relatively closely spaced APs, the ADP of each AP appears to still be present at the time of the next AP so that this next AP starts from a higher base) (Figure S1A, right, and Figure S1B), and the entirety of the slow, large, putatively calcium-based depolarizations that often follow a burst of APs (and that together make a CS) (Figure S1C). To handle all these cases using a single approach, we began by noting that these depolarizations (1) were always preceded by an AP and (2) all had a decay timescale of ~20 ms (Kandel and Spencer, 1961). We advanced through each AP beginning with the first one. For a given AP, considered to be the “starting AP” of this suprathreshold event, we took the minimum V_m value between 3 ms before the AP peak and the peak (which is thus clearly a subthreshold V_m level) and extended a horizontal line from that value until it again crossed the trace for the first time (but skipping past any crossing that occurred right after the AP due to a sharp, transient after-hyperpolarization). The beginning of the horizontal line was considered the “start time” of the suprathreshold event. We then determined the “end time” of the event based on several factors. We considered the end of the horizontal line to be “tentative end time (a).” We checked all APs (if there were any) whose peaks occurred within the interval defined by the horizontal line. Generally, we considered the event to continue as long as each successive AP had a higher threshold than the previous one. Specifically, if the thresholds of a successive pair of APs decreased and the latter AP’s threshold came within 5 mV of the “starting AP”’s threshold, then the time of the minimum V_m between 3 ms before that latter AP’s peak and the peak was considered to be “tentative end time (b).” This allowed decreasing thresholds within a longer CS, as long as the underlying depolarization was high enough to justify considering those APs as still being within the CS. Also, if two successive AP peaks occurred >25 ms apart and the latter AP’s threshold was higher but within 5 mV of the “starting AP”’s threshold, then the time of the minimum V_m between 3 ms before that latter AP’s peak and the peak was considered to be “tentative end time (c).” This handled cases where simple variability caused successive, relatively widely spaced APs to have slightly increasing thresholds. Separately, we removed all APs and spikelets within the interval defined by the horizontal line by removing intervals from the minimum V_m between 3 ms before the peak and the peak, to the minimum V_m between the peak and 5 ms after the peak of each AP or spikelet. Then we linearly interpolated across the resulting gaps to give an interpolated trace for this event. The interpolated trace was binned into 5 ms bins, and we looked for the first time the binned trace decreased monotonically for ≥ 20 ms and ended within 5 mV of the “starting AP”’s threshold. If no such drop existed, we looked for the longest existing monotonic drop ending within 5 mV of the “starting AP”’s threshold. We considered the time of the minimum V_m within the last bin of the monotonic drop to be “tentative end time (d),” where the last bin was allowed to extend past the original 20 ms decrease or the end of the horizontal line in order to capture the entire slow decay. (In a small number of special cases, there were no decreases between successive bins, so the “tentative end time (d)” was taken from within the last bin.) The idea was that suprathreshold events generally end with a smooth decay of ≥ 20 ms that returns close to the “starting AP”’s threshold, with shorter decays allowed for shorter events (e.g., single APs versus CSs) where repolarization may not be strong enough to overwhelm subsequent input for a full ~20 ms. We then set the event’s end time to be the earliest of the tentative end times (b–d). If it was (b) or (c), the end time was revised by setting it to the time of the minimum V_m in the last 5 ms bin between the two successive APs that had dropped from the previous bin. We then moved on to the first AP after the end time; this became the new “starting AP.” When the last AP was reached, the V_m between the start and end time of each event was removed and the trace linearly interpolated across the gaps to yield the subthreshold V_m trace. The mean of the subthreshold trace as a function of the animal’s location for a given head direction was binned in the same way as the AP firing rate in the “Place Field Classification” section to give the subthreshold field. Finally, we note the effect of the small hyperpolarizing holding current applied to some of the cells during awake recording. This would tend to hyperpolarize the V_m by $\sim R_N \times$ the holding current. To check that the results (Figures 4B–4G) were probably not affected by this, we estimated what the subthreshold values would have

been if no holding current was applied but kept the AP thresholds the same to make a conservative comparison (though one would actually expect thresholds to rise along with V_m based on Figure S1D and thus keep all the results “in register”). The results were unchanged: baseline V_m (place: -65.1 ± 2.2 mV versus silent: -58.2 ± 2.3 mV; $p = 0.056$), peak subthreshold V_m (-52.3 ± 2.4 versus -55.2 ± 2.2 mV; $p = 0.38$), threshold – baseline (9.3 ± 1.3 versus 10.9 ± 1.2 mV; $p = 0.38$), peak – baseline (12.8 ± 2.8 versus 2.9 ± 0.3 mV; $p = 0.024$, unchanged because both values were corrected by the same amount), peak – threshold (3.5 ± 1.7 versus -7.9 ± 1.1 mV; $p = 0.00072$).

Complex-Spike Classification

To classify an event as a CS, we started with the interpolated trace for a given event (in which the fast events, i.e., APs and spikelets, but not the slow depolarization, were eliminated) taken from the “[Determination of Subthreshold Field](#)” section. We considered the trace starting from the beginning of the horizontal line and ending at the determined end time. We measured the amplitude from the horizontal line to the peak of the interpolated trace, measured the width of the interpolated trace at the V_m halfway between the horizontal line and the peak (crossing any transient dips between the outermost limits), and computed the product of this amplitude and width. For each cell, we set three thresholds for amplitude, width, and amplitude \times width, and classified those events that satisfied all three thresholds to be CSs. The thresholds were ~ 15 mV, ~ 25 ms, and $\sim 15 \times 25$ mV \times ms, respectively, adjusted manually based on visual inspection of the resulting classification. A few events classified as CSs were rejected upon manual inspection. For determining the location at which a CS occurred, we set the time of occurrence to be that of the peak of the first AP in the CS.

Determination of Complex-Spike Plateau Level

The V_m reached by the slow, large depolarization of each CS was determined as follows. Intervals from the minimum V_m between 3 ms before the peak and the peak, to the minimum V_m between the peak and 5 ms after the peak of each AP or spikelet were removed from the CS’s V_m trace, linear interpolation was applied across the resulting gaps, the interpolated trace was low-pass-filtered with high cutoff 20 Hz, then the peak was taken from this smoothed trace. [Figure S2A](#) shows the distribution of these values for all CSs from all place and silent cells (mean \pm SD = -24.2 ± 4.4 mV). The mean plateau level of all CSs from a given cell was consistent across place, silent, active, and nonactive cells (mean \pm SD = -24.1 ± 2.8 mV) (only one silent cell and no additional nonactive cells had CSs). This mean plateau level and the baseline V_m were uncorrelated ($p = -0.12$; $p = 0.76$; regression line: mean CS plateau level = $-0.078 \times$ baseline $V_m - 29.0$ mV), and the mean plateau level and AP threshold were uncorrelated ($p = 0.41$; $p = 0.27$; mean CS plateau level = $0.26 \times$ AP threshold – 10.4 mV) across cells.

Pre-exploration Bursting Quantification

Immediately upon breaking into the neuron and achieving the whole-cell recording configuration, while the animal was anesthetized, we injected a series of depolarizing current steps. For each step, the current started at 0 nA, lasted for 300 ms, then returned to zero. The first depolarizing step was 0.1 or 0.2 nA and was increased in increments of 0.1 or 0.2 nA, respectively, for successive steps. The firing pattern of the first step that evoked ≥ 5 APs was used to determine the propensity to burst and is shown for each cell in [Figure 5](#). The degree of bursting was defined as the fraction of all APs in the firing pattern that occurred in bursts of ≥ 2 APs with ISIs ≤ 10 ms. An exception was made for cell 1 which (1) fired some spontaneous APs, thus for that cell the first step value that evoked a consistent firing pattern was used, and (2) displayed a CS-like burst at the beginning of each step of 0.2 nA or more, thus the APs in that burst were counted as bursts even though the ISIs were > 10 ms.

SUPPLEMENTAL INFORMATION

Supplemental Information includes two figures and Supplemental Experimental Procedures and can be found with this article online at doi:10.1016/j.neuron.2011.03.006.

ACKNOWLEDGMENTS

We would like to thank Brigitte Geue, Rüdiger Karpinski, and Arnold Stern at Humboldt University for technical assistance, and Joshua Dudman and Jeffrey Magee for valuable discussions. This work was supported by Neurocure, Bernstein Center for Computational Neuroscience (BMBF), Humboldt University, and Neuro-behavior ERC grants (M.B.); INSERM, Agence Nationale de la Recherche (grant ANR-09-BLAN-0259-01), and a Human Frontier Science Program Long Term Fellowship (J.E.); and the Howard Hughes Medical Institute and a European Molecular Biology Organization Long Term Fellowship (A.K.L.).

Accepted: February 25, 2011

Published: April 13, 2011

REFERENCES

- Andersen, P., Morris, R., Amaral, D., Bliss, T., and O’Keefe, J., eds. (2007). *The Hippocampus Book* (New York: Oxford University Press).
- Azouz, R., and Gray, C.M. (2003). Adaptive coincidence detection and dynamic gain control in visual cortical neurons *in vivo*. *Neuron* 37, 513–523.
- Davidson, T.J., Kloosterman, F., and Wilson, M.A. (2009). Hippocampal replay of extended experience. *Neuron* 63, 497–507.
- de Almeida, L., Idiart, M., and Lisman, J.E. (2009). The input-output transformation of the hippocampal granule cells: From grid cells to place fields. *J. Neurosci.* 29, 7504–7512.
- Dragoi, G., and Tonegawa, S. (2011). Preplay of future place cell sequences by hippocampal cellular assemblies. *Nature* 469, 397–401.
- Epsztein, J., Lee, A.K., Choref, E., and Brecht, M. (2010). Impact of spikelets on hippocampal CA1 pyramidal cell activity during spatial exploration. *Science* 327, 474–477.
- Fenton, A.A., Kao, H.Y., Neymotin, S.A., Olypher, A., Vayntrub, Y., Lytton, W.W., and Ludvig, N. (2008). Unmasking the CA1 ensemble place code by exposures to small and large environments: More place cells and multiple, irregularly arranged, and expanded place fields in the larger space. *J. Neurosci.* 28, 11250–11262.
- Figenschou, A., Hu, G.Y., and Storm, J.F. (1996). Cholinergic modulation of the action potential in rat hippocampal neurons. *Eur. J. Neurosci.* 8, 211–219.
- Frank, L.M., Stanley, G.B., and Brown, E.N. (2004). Hippocampal plasticity across multiple days of exposure to novel environments. *J. Neurosci.* 24, 7681–7689.
- Fraser, D.D., and MacVicar, B.A. (1996). Cholinergic-dependent plateau potential in hippocampal CA1 pyramidal neurons. *J. Neurosci.* 16, 4113–4128.
- Frick, A., Magee, J., and Johnston, D. (2004). LTP is accompanied by an enhanced local excitability of pyramidal neuron dendrites. *Nat. Neurosci.* 7, 126–135.
- Gasparini, S., Migliore, M., and Magee, J.C. (2004). On the initiation and propagation of dendritic spikes in CA1 pyramidal neurons. *J. Neurosci.* 24, 11046–11056.
- Gelbard-Sagiv, H., Mukamel, R., Harel, M., Malach, R., and Fried, I. (2008). Internally generated reactivation of single neurons in human hippocampus during free recall. *Science* 322, 96–101.
- Hafting, T., Fyhn, M., Molden, S., Moser, M.B., and Moser, E.I. (2005). Microstructure of a spatial map in the entorhinal cortex. *Nature* 436, 801–806.
- Harris, K.D., Hirase, H., Leinekugel, X., Henze, D.A., and Buzsáki, G. (2001). Temporal interaction between single spikes and complex spike bursts in hippocampal pyramidal cells. *Neuron* 32, 141–149.
- Harvey, C.D., Collman, F., Dombeck, D.A., and Tank, D.W. (2009). Intracellular dynamics of hippocampal place cells during virtual navigation. *Nature* 461, 941–946.
- Hill, A.J. (1978). First occurrence of hippocampal spatial firing in a new environment. *Exp. Neurol.* 62, 282–297.

- Jensen, M.S., Azouz, R., and Yaari, Y. (1996). Spike after-depolarization and burst generation in adult rat hippocampal CA1 pyramidal cells. *J. Physiol.* 492, 199–210.

Jia, H., Rochefort, N.L., Chen, X., and Konnerth, A. (2010). Dendritic organization of sensory input to cortical neurons in vivo. *Nature* 464, 1307–1312.

Kamondi, A., Acsády, L., Wang, X.J., and Buzsáki, G. (1998). Theta oscillations in somata and dendrites of hippocampal pyramidal cells in vivo: activity-dependent phase-precession of action potentials. *Hippocampus* 8, 244–261.

Kandel, E.R., and Spencer, W.A. (1961). Electrophysiology of hippocampal neurons. II. After-potentials and repetitive firing. *J. Neurophysiol.* 24, 243–259.

Karlsson, M.P., and Frank, L.M. (2008). Network dynamics underlying the formation of sparse, informative representations in the hippocampus. *J. Neurosci.* 28, 14271–14281.

Kentros, C., Hargreaves, E., Hawkins, R.D., Kandel, E.R., Shapiro, M., and Muller, R.V. (1998). Abolition of long-term stability of new hippocampal place cell maps by NMDA receptor blockade. *Science* 280, 2121–2126.

Lee, A.K., Manns, I.D., Sakmann, B., and Brecht, M. (2006). Whole-cell recordings in freely moving rats. *Neuron* 51, 399–407.

Lee, A.K., Epsztein, J., and Brecht, M. (2009). Head-anchored whole-cell recordings in freely moving rats. *Nat. Protoc.* 4, 385–392.

Leutgeb, S., Leutgeb, J.K., Treves, A., Moser, M.B., and Moser, E.I. (2004). Distinct ensemble codes in hippocampal areas CA3 and CA1. *Science* 305, 1295–1298.

Leutgeb, S., Leutgeb, J.K., Barnes, C.A., Moser, E.I., McNaughton, B.L., and Moser, M.B. (2005). Independent codes for spatial and episodic memory in hippocampal neuronal ensembles. *Science* 309, 619–623.

Long, M.A., Jin, D.Z., and Fee, M.S. (2010). Support for a synaptic chain model of neuronal sequence generation. *Nature* 468, 394–399.

Losonczy, A., Makara, J.K., and Magee, J.C. (2008). Compartmentalized dendritic plasticity and input feature storage in neurons. *Nature* 452, 436–441.

Margrie, T.W., Brecht, M., and Sakmann, B. (2002). In vivo, low-resistance, whole-cell recordings from neurons in the anaesthetized and awake mammalian brain. *Pflugers Arch.* 444, 491–498.

Mathy, A., Ho, S.S., Davie, J.T., Duguid, I.C., Clark, B.A., and Häusser, M. (2009). Encoding of oscillations by axonal bursts in inferior olive neurons. *Neuron* 62, 388–399.

McHugh, T.J., Blum, K.I., Tsien, J.Z., Tonegawa, S., and Wilson, M.A. (1996). Impaired hippocampal representation of space in CA1-specific NMDAR1 knockout mice. *Cell* 87, 1339–1349.

McNaughton, B.L., Battaglia, F.P., Jensen, O., Moser, E.I., and Moser, M.B. (2006). Path integration and the neural basis of the ‘cognitive map’. *Nat. Rev. Neurosci.* 7, 663–678.

Mehta, M.R., Quirk, M.C., and Wilson, M.A. (2000). Experience-dependent asymmetric shape of hippocampal receptive fields. *Neuron* 25, 707–715.

Moore, S.J., Cooper, D.C., and Spruston, N. (2009). Plasticity of burst firing induced by synergistic activation of metabotropic glutamate and acetylcholine receptors. *Neuron* 61, 287–300.

Muller, R.U., and Kubie, J.L. (1987). The effects of changes in the environment on the spatial firing of hippocampal complex-spike cells. *J. Neurosci.* 7, 1951–1968.

O’Keefe, J., and Burgess, N. (2005). Dual phase and rate coding in hippocampal place cells: Theoretical significance and relationship to entorhinal grid cells. *Hippocampus* 15, 853–866.

O’Keefe, J., and Conway, D.H. (1978). Hippocampal place units in the freely moving rat: why they fire where they fire. *Exp. Brain Res.* 31, 573–590.

O’Keefe, J., and Dostrovsky, J. (1971). The hippocampus as a spatial map. Preliminary evidence from unit activity in the freely-moving rat. *Brain Res.* 34, 171–175.

O’Keefe, J., and Nadel, L. (1978). *The Hippocampus as a Cognitive Map* (Oxford: Clarendon Press).

Oh, M.M., Kuo, A.G., Wu, W.W., Sametsky, E.A., and Disterhoft, J.F. (2003). Watermaze learning enhances excitability of CA1 pyramidal neurons. *J. Neurophysiol.* 90, 2171–2179.

Quiroga, R.Q., Reddy, L., Kreiman, G., Koch, C., and Fried, I. (2005). Invariant visual representation by single neurons in the human brain. *Nature* 435, 1102–1107.

Ranck, J.B., Jr. (1973). Studies on single neurons in dorsal hippocampal formation and septum in unrestrained rats. I. Behavioral correlates and firing repertoires. *Exp. Neurol.* 47, 461–531.

Sjöström, P.J., and Nelson, S.B. (2002). Spike timing, calcium signals and synaptic plasticity. *Curr. Opin. Neurobiol.* 12, 305–314.

Solstad, T., Moser, E.I., and Einevoll, G.T. (2006). From grid cells to place cells: a mathematical model. *Hippocampus* 16, 1026–1031.

Staff, N.P., Jung, H.Y., Thiagarajan, T., Yao, M., and Spruston, N. (2000). Resting and active properties of pyramidal neurons in subiculum and CA1 of rat hippocampus. *J. Neurophysiol.* 84, 2398–2408.

Suzuki, T., Kodama, S., Hoshino, C., Izumi, T., and Miyakawa, H. (2008). A plateau potential mediated by the activation of extrasynaptic NMDA receptors in rat hippocampal CA1 pyramidal neurons. *Eur. J. Neurosci.* 28, 521–534.

Takahashi, H., and Magee, J.C. (2009). Pathway interactions and synaptic plasticity in the dendritic tuft regions of CA1 pyramidal neurons. *Neuron* 62, 102–111.

Thompson, L.T., and Best, P.J. (1989). Place cells and silent cells in the hippocampus of freely-behaving rats. *J. Neurosci.* 9, 2382–2390.

Thompson, L.T., and Best, P.J. (1990). Long-term stability of the place-field activity of single units recorded from the dorsal hippocampus of freely behaving rats. *Brain Res.* 509, 299–308.

Traub, R.D., and Llinás, R. (1979). Hippocampal pyramidal cells: Significance of dendritic ionic conductances for neuronal function and epileptogenesis. *J. Neurophysiol.* 42, 476–496.

Waydo, S., Kraskov, A., Quiroga, R., Fried, I., and Koch, C. (2006). Sparse representation in the human medial temporal lobe. *J. Neurosci.* 26, 10232–10234.

Wilson, M.A., and McNaughton, B.L. (1993). Dynamics of the hippocampal ensemble code for space. *Science* 261, 1055–1058.

Wong, R.K., and Prince, D.A. (1978). Participation of calcium spikes during intrinsic burst firing in hippocampal neurons. *Brain Res.* 159, 385–390.

Zhang, W., and Linden, D.J. (2003). The other side of the engram: Experience-driven changes in neuronal intrinsic excitability. *Nat. Rev. Neurosci.* 4, 885–900.